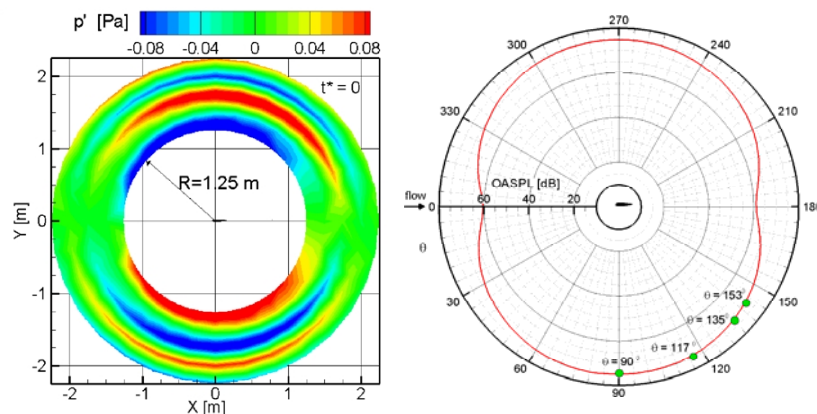




Executive summary

Aeroacoustic analysis of a rod-airfoil flow by means of time-resolved PIV



Left: Predicted wave fronts that are emanating from the airfoil

Right: Predicted directivity pattern, green dots represent measurements

Problem area

The present paper investigates the feasibility of prediction of vortex-structure noise based on time resolved Particle Image Velocimetry (PIV). We consider the case of an airfoil immersed in the wake of a cylindrical rod.

Description of work

By PIV the flow field around the airfoil is measured. The pressure field can then be obtained as a solution of the Poisson equation. Subsequently, the pressure at the airfoil surface is used as source term in Curle's analogy to predict the sound emission. Furthermore, an alternative approach based on integral aerodynamic loads is followed, which exploits the fact the airfoil can be considered to be

compact body. The results of the aeroacoustic predictions are compared with microphone measurements which were acquired during the experiment.

Results and conclusions

Both approaches give results that are in good agreement with the microphone measurements at the tone corresponding to the Karman vortex shedding frequency.

Applicability

The results demonstrate that sound determination based on PIV is viable. The next step is to extend the method to broadband noise prediction.

Report no.

NLR-TP-2009-440

Author(s)

V. Lorenzoni
P. Moore
F. Scarano
M. Tuinstra

Report classification

UNCLASSIFIED

Date

20 August 2009

Knowledge area(s)

Aëro-akoestisch en experimenteel
aërodynamisch onderzoek

Descriptor(s)

Rod-Airfoil
PIV
Sound
Acoustic Analogy
Curle's Analogy

Nationaal Lucht- en Ruimtevaartlaboratorium, National Aerospace Laboratory NLR

Anthony Fokkerweg 2, 1059 CM Amsterdam,
P.O. Box 90502, 1006 BM Amsterdam, The Netherlands

Telephone +31 20 511 31 13, Fax +31 20 511 32 10, Web site: www.nlr.nl



NLR-TP-2009-440

Aeroacoustic analysis of a rod-airfoil flow by means of time-resolved PIV

V. Lorenzoni¹, P. Moore¹, F. Scarano¹ and M. Tuinstra

¹ TU Delft



This report is based on a presentation held at 15th AIAA/CEAS Aeroacoustic Conference, Miami, Florida, 11-13 May 2009.

The contents of this report may be cited on condition that full credit is given to NLR and the authors.

This publication has been refereed by the Advisory Committee AEROSPACE VEHICLES.

Customer National Aerospace Laboratory NLR
Contract number ----
Owner National Aerospace Laboratory NLR + partner(s)
Division NLR Aerospace Vehicles
Distribution Unlimited
Classification of title Unclassified
January 2010

Approved by:

| Author | Reviewer | Managing department |
|--|------------|--|
|  11-02-2010 | fo 11/2/10 |  16/2 |

Contents

| | |
|-------------------------------|-----------|
| Nomenclature | 3 |
| I Introduction | 4 |
| II Aeroacoustic model | 4 |
| III Experiment | 5 |
| IV Acoustic prediction | 10 |
| V Conclusion | 13 |
| Acknowledgements | 14 |
| References | 14 |

Aeroacoustic analysis of a rod-airfoil flow by means of time-resolved PIV

Lorenzoni V.,* Moore P.,[†] Scarano F.[‡]

Delft University of Technology, Aerospace Engineering Department, Delft, 2629 HS, The Netherlands

Tuinstra M.[§]

Dutch National Aerospace Laboratory NLR, 8316 PR, Marknesse, The Netherlands

The present study investigates an experimental approach for aeroacoustic prediction of vortex-structure noise based on time-resolved Particle Image Velocimetry (TR-PIV). The test configuration consists of a NACA0012 airfoil immersed in the wake of an cylindrical rod. The velocity field around the airfoil measured by the PIV experiment is used to evaluate the corresponding pressure field as solution of the planar Poisson equation for the pressure. The resulting pressure evaluated at the airfoil surface constitutes the source term of the implemented Curle's aeroacoustic analogy. An alternative formulation based on the integral aerodynamic loads is also followed. The results of the aeroacoustic prediction are compared with microphone measurements conducted simultaneously, in terms of spectra and directivity pattern. The results show a good agreement with the microphone measurements for the evaluation of the tonal component corresponding to the frequency of interaction of the Kármán vortices with the airfoil leading edge.

Nomenclature

| | |
|---------------------------|---|
| St | Strouhal number |
| Re | Reynolds number |
| \mathbf{y} | Acoustic source position [m] |
| \mathbf{x} | Listener position [m] |
| δ_{ij} | Kronecker delta |
| t_e | Retarded time |
| r | Distance between generic surface point and listener position |
| R | Distance between airfoil leading edge and listener position |
| p_0 | Atmospheric pressure [Pa] |
| p' | Pressure fluctuation $p - p_0$ [Pa] |
| c_0 | Speed of sound [m/s] |
| $\langle f(x, t) \rangle$ | Local time average |
| f_{fluct} | Local time fluctuation $f(x, y, t) - \langle f(x, t) \rangle$ |
| rms | Root mean square value |
| SPL | Sound pressure level [Pa] |
| $OASPL$ | Overall sound pressure level [Pa] |
| $C.L.$ | Correlation length [% of span] |
| T_{shed} | Shedding period [s] |
| t^* | Normalized time [t/T_{shed}] |
| CV | Control volume for evaluation of aerodynamic loads |
| LE | Airfoil leading edge |

*Research Assistant, Aerodynamic Section

[†]Researcher, Aerodynamic Section

[‡]Professor, Aerodynamic Section

[§]NLR Researcher, Dutch National Aerospace Laboratory NLR.

I. Introduction

VORTEX-STRUCTURE interaction noise is become of main concern in aeronautics as well as in various industrial environments. Several devices are arranged in such a way that downstream bodies are embedded in the wake of upstream bodies. This is typically the case of a bank of heat exchanger tubes, rotor stator configurations of turbo-engines, ventilating systems and helicopter rotors in case of vortex-blade interaction. The rod-airfoil configuration as test case of combined vortex shedding noise and turbulence-structure interaction noise was proposed by Jacobs¹ as benchmark test configuration of numerical CFD codes (URANS, LES) for broadband noise predictions. Casalino² applied URANS simulations for the characterization of the flow field on the same configuration and developed an advanced-time numerical code for noise prediction based on Ffowcs Williams-Hawkings equation. Numerical investigations on the same configuration have been performed inside the framework of European Project PROBAND.³ The results obtained by the application of several computational aeroacoustic (CAA) techniques have been compared with experimental measurements for the assessment on the broadband noise prediction.

To the knowledge of the authors, the time-resolved PIV technique for quantitative aeroacoustic prediction on the rod-airfoil configuration has not been explored yet. Recent improvements of velocimetry techniques over the last two decades in terms of spatial and temporal resolution, have opened the possibility of using experimental PIV data for aeroacoustic purposes. In particular, the use of time-resolved PIV (TR-PIV) data in aeroacoustics was first proposed by Seiner^{4,5} in devising a new methodology for jet noise reduction, using a statistical reformulation of Lighthill's analogy developed by Goldstein.⁶ Recently Wernet⁷ performed TR-PIV experiments at high repetition rate on the shear layer of hot and cold jets for evaluation of the two-point delayed correlation tensor of the velocity. Schröder *et al.*⁸ performed simultaneous PIV and acoustic measurements on the trailing edge of a flat board at high recording rate for detection of the statistical flow features responsible for the noise emission and the evaluation of the source terms of Howe's formulation⁹ for the trailing edge emission. Henning¹⁰ *et al.* have recently performed PIV experiment and simultaneous microphone measurements on a circular cylinder and inside a leading edge slat to calculate the cross-correlation between the velocity/vorticity field and the acoustic pressure, for statistical detection of the flow structures responsible for the noise emission. A different approach for PIV based aeroacoustic predictions was followed by Schram¹¹ analyzing the vortex pairing noise due to acoustically driven instabilities in the shear layer of a subsonic jet. In this case phase-locking of the jet instability allowed for the phase-resolved description of the vortex pairing. The evaluation of the aeroacoustic sources was obtained by a conservative formulation of Vortex Sound Theory^{12,13} for homentropic, low Mach number axisymmetrical free flows. The robustness of the integral formulation based on conservation of the flow invariants, provided a good agreement of the noise prediction obtained by PIV data with respect to analytical models.

The mentioned studies were all based on the kinematic properties of the flows with no direct attempt toward the determination of the instantaneous pressure spatial distribution. In this work the acoustic computation hinges on the implementation of Curle's aeroacoustic analogy in a distributed and an integral formulation. Both the approaches require the knowledge of the unsteady pressure for evaluation of the acoustic sources. The pressure field is calculated by numerical integration of the pressure gradient directly obtained from the momentum conservation law. A similar approach has been lately applied by Haigermoser¹⁴ to a cavity flow using planar TR-PIV in a water flow experiment in combination with a pressure reconstruction algorithm and Curle's analogy. The reliability of the acoustic prediction based on such a method still needed to be tested in terms of magnitude of the spectra by comparison with microphone measurements. The scope of the present work is to quantitatively demonstrate, within the technical limits of this specific experiment, the feasibility of using time-resolved PIV experimental data for the aeroacoustic noise prediction in vortex-structure-interaction problems.

II. Aeroacoustic model

An extension to Lighthill's aeroacoustic analogy¹⁵ to account for the presence of solid bodies inside the flow domain, was developed by Curle.¹⁶ The analytical formulation of Curle's analogy for low Mach number flows and compact geometries can be rewritten as

$$p'(\mathbf{x}, t) = -\frac{x_j}{4\pi c_0 |\mathbf{x}|} \frac{\partial}{\partial t} \int_{\partial V_y} \frac{p' \delta_{ij}}{r} \Big|_{t=t_e} n_i dS, \quad (1)$$

where the quantity $p' = p - p_0$ indicates the pressure fluctuation with respect to the atmospheric reference pressure p_0 . The quantity on the left hand side represents the propagating acoustic pressure while p' inside the integral indicates the pressure fluctuation at the body surface induced by the flow dynamics, which is identified as the source of noise. The quadrupolar term and the viscous dipoles have been neglected because of the low Mach number and relatively high Reynolds number of the flow and the acoustic compactness of the airfoil.¹⁷ The subscript $t = t_e$ indicates that the pressure fluctuations at the surface have to be evaluated at the retarded time $t_e = t - \frac{r}{c_0}$.

An alternative approach for noise prediction in case of compact geometries is based on the evaluation of the time variations of the integral aerodynamic loads acting on the immersed body (Gutin's principle⁶). For bodies small compared to the acoustic wavelength it is possible to neglect the retarded time variations between different points on the integration surface. The surface integral of the pressure in equation (1) then corresponds to the instantaneous lift and drag forces acting on the airfoil section, which have been calculated by integrating the momentum equation on a control volume (surface) surrounding the airfoil, following the approach reported by Kurtulus *et al.*¹⁸

The instantaneous pressure field needed for the evaluation of the source terms in both the analogy formulations is calculated by exploiting the Planar Pressure Imaging (PPI) technique.¹⁹ The pressure gradient of the Navier-Stokes equations are obtained from TR-PIV data using the definition of substantial acceleration disregarding the viscous contribution, following the method adopted by Liu and Katz.²⁰ Application of the divergence operator to the planar components of pressure gradient leads to the 2D Poisson equation for the pressure

$$\nabla^2 p = -\rho \left(\frac{\partial}{\partial x} \frac{Du}{Dt} + \frac{\partial}{\partial y} \frac{Dv}{Dt} \right). \quad (2)$$

Equation (2) has been solved using a numerical algorithm reported by de Kat *et al.*,²¹ in the assumption of incompressible flow. Validation of the method using 3D flow data is currently being investigated.

III. Experiment

III.A. Experimental setup

Combined PIV and acoustic experiments were carried out in the small anechoic wind tunnel (KAT) of the Dutch "National Aerospace Laboratories" NLR. The anechoic chamber dimension is $5.5 \times 5.5 \times 2.5 \text{ m}^3$ and it is covered with 0.5 m long foam wedges, yielding 99 % acoustic absorption above 500 Hz . The wind tunnel has an open test section with exit dimensions of $0.51 \times 0.38 \text{ m}^2$. A cylindrical rod of 6 mm diameter was vertically mounted 22 cm downstream of the wind tunnel exit. A NACA0012 Plexiglas airfoil, with a chord of 10 cm , was vertically placed in the wake of the rod at zero incidence. The rod and airfoil were placed at a relative distance of 10.2 cm . The configuration was examined for a nominal free-stream velocity of 15 m/s with incoming turbulence level of 0.5% at the centerline.

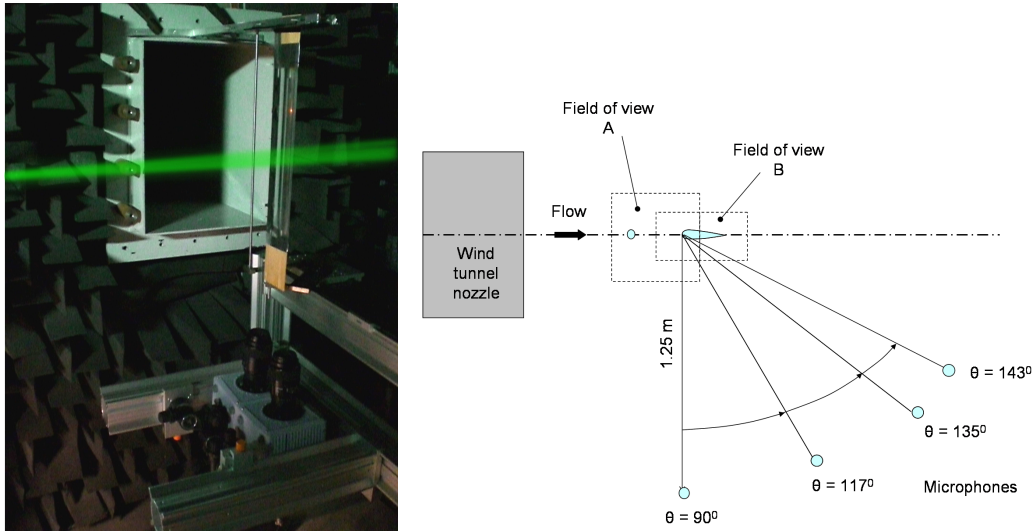


Figure 1. PIV experimental setup (left) and schematic of the PIV fields of view and microphone disposition (right)

Two-component time-resolved particle image velocimetry (TR-PIV) was used to obtain planar velocity field measurements around the airfoil. The light sheet was placed at the middle span section of the airfoil. The transparent material of the airfoil allowed the simultaneous measurement of the flow-field on both sides of the airfoil, except for two small regions at the airfoil edges. Two CMOS cameras were combined to image the flow around the airfoil at relatively high spatial resolution. These were mounted next to each other underneath the airfoil as shown in Figure 1 (left). Each camera was equipped with a Nikon objective with a focal length of 105 mm and numerical aperture set to $f\# = 2.8$. The synchronization between laser and cameras was performed by means of a LaVision High-Speed controller and the acquisition was controlled by a PC with the DAVIS 7.2 software.

The Reynolds number was 6,000 and 100,000 with respect to the rod diameter and the airfoil chord respectively. Two fields of view (FOV) have been examined, indicated in the sketch of Figure 1 as FOV-A and FOV-B respectively. The PIV measurement parameters relative to the main experiment (FOV-B) are shown in Table 1

Table 1. PIV measurement parameters

| | |
|-----------------------|---|
| Seeding material | smoke particles $\approx 1\mu\text{m}$ diameter |
| Illumination | Quantronix Nd-YLF 2x12 mJ @ 2700 Hz |
| Recording device | 2 x Photron Fast CAM SA1 CMOS cameras 12-bit (1024x1024 pixels, 20 μm pixel pitch) |
| Recording method | double frame/single exposure |
| Recording lens | $f = 105\text{ mm}$, $f\# = 2.8$ |
| Acquisition frequency | 2700 Hz double-pulsed mode |
| Combined sensor size | 1939 x 1024 px (FOV 164 x 83 mm^2) |
| Interrogation window | 21 x 21 px |
| Overlap | 75 % |
| Pulse separation | 50 μs |

The acoustic measurement system consisted of a set of four far-field LinearX-M51 microphones. These were placed at a fixed radius of 1.25 m from the airfoil leading edge at an angle, with respect to the airfoil

chord of 90° , 117° , 135° , 143° as shown in the sketch of Figure 1 (right), at the height of the airfoil midspan. The microphone recordings were taken simultaneously with the PIV measurements. Table 2 summarizes the characteristics of the acoustic measurement system.

Table 2. Acoustic measurement characteristics

| | |
|---------------------------------|--|
| Number of far-field microphones | 4 |
| Angular positions | $90^\circ, 117^\circ, 135^\circ, 143^\circ$ |
| Distance from the airfoil | 1.25 m |
| Microphone type | LinearX-M51, omnidirectional pressure microphone |
| Acquisition system | GBM-Viper |
| Sample frequency | 51.2 kHz |
| Measuring time | 20 s |
| Frequency resolution | 12.5 Hz |

III.B. Planar PIV measurements

An overview of the Kármán vortex street behind the rod and the interaction of vortical structures with the airfoil LE is provided by FOV-A (Figure 2-left). The detailed visualization of the flow around the entire airfoil is possible in FOV-B, which is needed for evaluation of whole aeroacoustic source. The velocity field from the PIV recordings was evaluated using the Window Deformation Iterative Multigrid algorithm (WIDIM) developed by Scarano and Riethmuller.²² The spatial resolution of the velocity field corresponded to 1.1 vector/mm (1.1 % chord) for FOV-A and 2.4 vectors/mm (0.4 % chord) for FOV-B. The maximum operational frequency of the PIV acquisition system at full frame resolution was limited to 2,700 Hz, which determined a time resolution of the velocity field of approximately 5 samples/shedding period.

Contours of the instantaneous vorticity field are visualized in Figure 2.

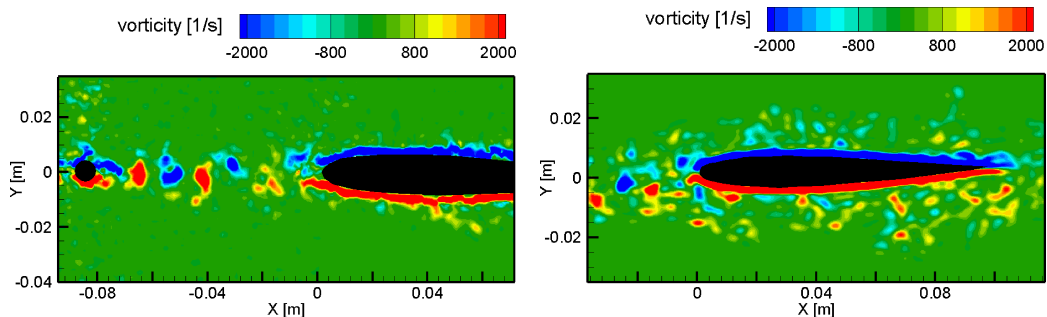


Figure 2. Instantaneous contours of the out-of-plane vorticity component. Low resolution Kármán wake (FOV-A, left) and high-resolution flow around the airfoil (FOV-B, right)

The Kármán wake consists of counter-rotating vortices almost aligned along the rod-airfoil symmetry line. Moving downstream the wake of the rod enlarges and the alternating vortices appear to progressively loose coherence due to the growth of three-dimensional instabilities. Nevertheless a clear periodicity upstream of the LE is maintained. Approaching the LE counter-clockwise rotating vortices tend to shift towards the lower side of the wake axis, conversely clockwise rotating vortices shift towards the upper side. In proximity of the LE vortices are accelerated towards one of the two sides.

A close up of the vortex-airfoil interaction process is provided by the right picture of Figure 2. The higher spatial resolution with respect to the left picture, allows to identify also the small-scale vortical structures present in the Kármán wake. These structures are reported to be responsible for the broadband component of the noise radiated by the configuration (see Jacobs¹). The dimensions of vortical blobs decrease during convection along the airfoil sides and the vorticity levels in the back of the airfoil reduce to approximately 60 % of the levels in the front. No periodic behavior of the flow can be observed at the TE within the

present measurements. Moreover, the well known laminar separation phenomenon occurring around this specific airfoil which leads to TE noise (see Roger^{23,24}), appears to be inhibited by the high turbulence level of the rod wake where the airfoil is immersed. The large red and blue stripes around the airfoil are due to saturation of the vorticity levels, which was needed for the visualization of the vortical structures surrounding the airfoil. The physical boundary layer on the airfoil cannot be captured with the present measurement resolution and the thickness of these stripes should not be taken as an indication of the boundary layer.

III.C. Instantaneous pressure distribution

The pressure field around the airfoil was calculated as solution of the 2D incompressible Poisson equation for the pressure (equation (2)), using an algorithm developed by de Kat²¹ based on a second order central difference scheme. Dirichlet boundary conditions are taken in the irrotational flow region away from the turbulent wake and are derived from the steady Bernoulli relation. The pressure gradient provided by the PIV measurement, is used as Neumann boundary condition in the rotational parts of the flow boundaries and on the airfoil surface.

Figure 3 shows a sequence of instantaneous vertical velocity fields (left) and the corresponding pressure fields (right) at subsequent normalized time t^* during approximately one shedding cycle. In order to highlight the unsteady behavior of the flow only the velocity and pressure temporal fluctuations around the local time average are shown, $v_{fluct}(x, y, t)$ and $p_{fluct}(x, y, t)$ respectively.

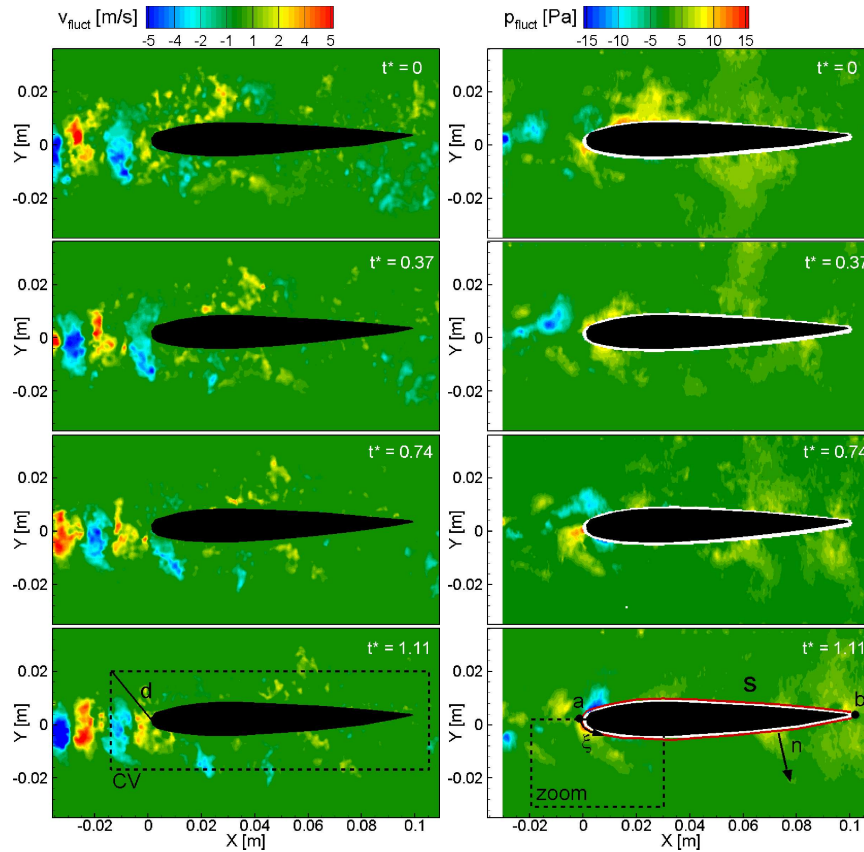


Figure 3. Time sequence of the instantaneous velocity fluctuations v_{fluct} and relative pressure fluctuations p_{fluct} at normalized times t^* (visualization every two snapshots). Control surface for aeroacoustic sources integration (bottom-right, red) and generic control volume CV for evaluation of the integral loads (bottom-left, dashed line)

The simultaneous visualization of velocity and pressure contours directly shows the relation between the flow pattern and the corresponding pressure distribution. The sequence of the vertical velocity fluctuations reveals the process of vortex convection and interaction with the airfoil LE also visualized in Figure 2. Close

alternating upward (red) followed by a downward (blue) velocity blobs indicate a clockwise rotating vortex. The vertical velocity fluctuations in the Kármán wake approaching the leading edge exhibit a magnitude of approximately 4 m/s ($27\% V_\infty$), whereas after the interaction with the airfoil such fluctuation levels decrease to less than 15% with respect to the free-stream velocity. During the interaction with the leading edge, larger vortical structures break down into smaller ones which convect along the airfoil sides. As the flow is accelerated along the first 20% of the airfoil chord the vortices undergo a prominent loss of coherence.

The pressure fluctuations upstream of the airfoil show a less clear pattern. Figure 3 (right), however, reveals a still distinguishable convection process of the local pressure fluctuations towards the LE and coherence loss at interaction with the airfoil. The cores of the coherent vortices embedded by close upward (red) and downward (blue) velocity bulges in Figure 3 (left), correspond to minima of the local pressure, as indicated by the low pressure (blue) regions of Figure 3 (right). Instead, relative maxima are attained at the saddle points formed between adjacent vortices. The levels of the pressure fluctuations oscillate between -15 and 15 Pa in the region in front of the airfoil and decrease more than 40 % behind the TE. The appearance of a similar pattern after about one shedding cycle in both the right and left sequences of Figure 3 qualitatively reveals that velocity and pressure fluctuations travel with the same convection velocity away from the object surface.

Figure 4 shows a more detailed view around the airfoil leading edge corresponding to the rectangular region indicated in the bottom right of Figure 3. Contours of the instantaneous pressure fluctuations are drawn together with vectors of the velocity fluctuations.

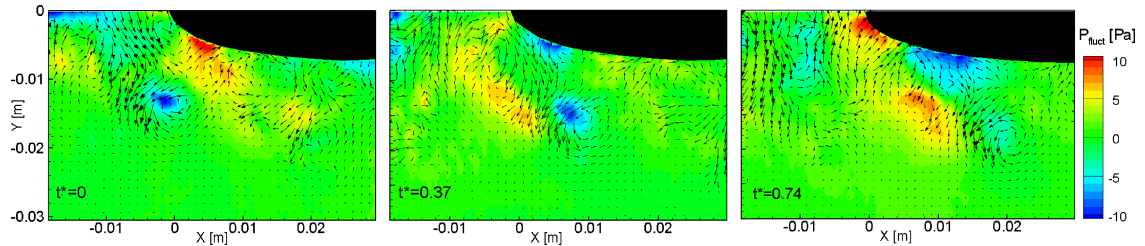


Figure 4. Sequence of instantaneous contours of pressure fluctuations and vectors of velocity fluctuations (visualization every two snapshots, 3rd vector in each dimension). Zoomed view around lower half of the airfoil leading edge

The flow-structure interaction process and the subsequent pressure build up at the airfoil surface is clearly visualized, which is of primary interest to the understanding of the noise generation mechanism. The Kármán vortices are deformed by interaction with the airfoil. The impingement of a vortex on the surface causes an increase of the local pressure while velocity components directed outward the airfoil surface induce a pressure decrease. The regions of higher velocity and the cores of the vortical structures correspond to pressure minima. The pressure fluctuations are convected along the side of airfoil and peak towards the airfoil surface. The overall interaction mechanism appears to weaken rapidly downstream.

The time varying pressure fluctuation p' , evaluated on the control surface (line) S approximating the physical airfoil surface (red line, bottom-right picture of Figure 3), is used as source term of Curle's aeroacoustic analogy given in equation (1). The instantaneous surface pressure fluctuation along the lower side of the control surface S is shown in a time-space diagram illustrated in Figure 5 (top). The distribution of the r.m.s. of the pressure fluctuations (σ_p) is shown in Figure 5 (bottom). The horizontal axis corresponds to the rectified local coordinate ξ along the lower side of the airfoil surface from point a to point b , indicated in the bottom right of Figure 3, normalized with the chord length (ξ/chord).

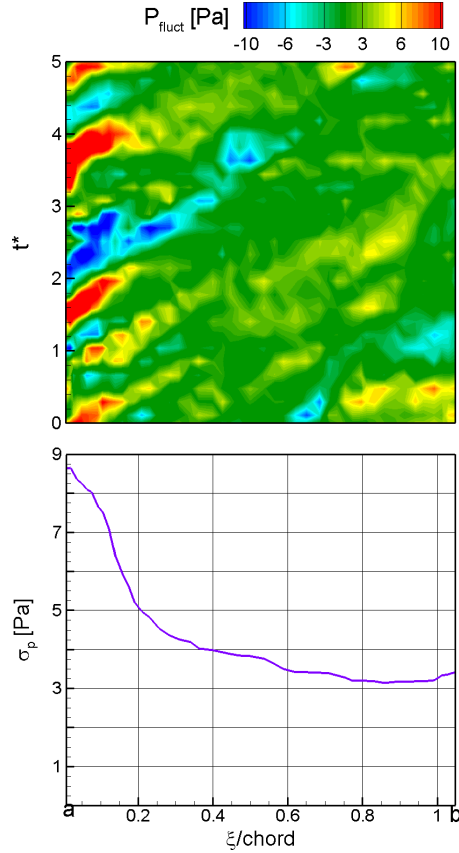


Figure 5. Time evolution of the pressure fluctuations (top) and r.m.s. value of the pressure (bottom) on a rectified coordinate along the lower side of integration surface S (from a to b).

The vertical axis in the top figure refers to a generic observation time normalized with the shedding period. The diagonal stripes are representative of convection of the pressure fluctuation along the lower side of the control surface. The inclination of the diagonal lines with respect to the vertical axis indicates a convection velocity of about 12 m/s . These stripes are spaced time-wise by one shedding cycle. The discontinuous appearance of the stripes is ascribed to uncertainty of the velocity measurement specifically at the solid surface. The r.m.s. of the pressure fluctuations in the bottom plot of Figure 5, calculated over 200 cycles along the same coordinate between point *a* and point *b*, gives an indication of the average spatial distribution of the fluctuation magnitude along the control surface S. The region of highest fluctuations is localized in the first 20 % of the airfoil chord. The intensity of fluctuations drops to less than 50% the peak value at half the chord. It is known that aerodynamic sound generation is caused by flow unsteadiness.¹⁵ This suggests that the LE region is that mostly responsible for the radiation of acoustic noise in the rod-airfoil configuration, confirming the previous results obtained by Jacobs.¹

IV. Acoustic prediction

The noise emitted by the airfoil was calculated as solution of equation (1) and its corresponding integral formulation, using a trapezoidal integration method for the surface integral and a forward difference scheme for time derivatives. The PIV experiment and the PPI reconstruction method used for the evaluation of the aeroacoustic sources, provided time-resolved 2D data relative to the midspan airfoil section. The 3D nature of the airfoil emission and the possible cancellation of acoustic sources along the span are accounted for by assuming that an equal in-phase emission occurs along a section of the span corresponding to a fraction of the physical span length. PIV measurements were performed in the spanwise direction on a window

corresponding to 25 % of the span length and revealed an almost in-phase impingement of the larger Kármán vortices for such observation window.²⁵ The correlation length, denoted as C.L. in the plots, is a percentage of the total span and indicates the effective reduced length used for the computation. C.L. 50% represents the case in which half of the airfoil span is considered giving effective contribution to the emission while 100% indicates that coherent phase emission is assumed along the whole airfoil span. The results provide a range of values in which C.L. = 50% represents the lower boundary and C.L.= 100% the upper boundary, the actual value is expected to be comprised between these boundaries. The computed spectra are compared with the measurement of the microphone perpendicular to the airfoil chord, indicated as $\theta = 90^\circ$ in the right sketch of Figure 1. All the spectra are calculated using a Welch algorithm and have 12.5 Hz resolution.

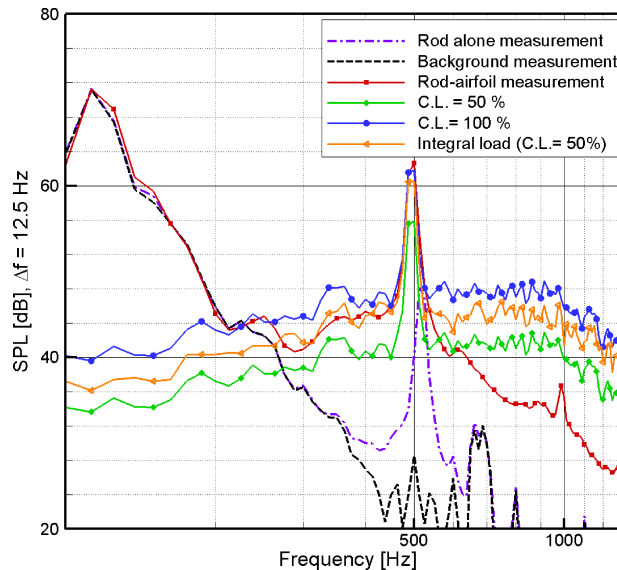


Figure 6. Measured spectra of the background noise, airfoil alone noise and rod-airfoil noise, computed spectra of rod-airfoil emission (C.L.= 50% and C.L.= 100%) and prediction based on integral loads formulation (C.L.= 50 %)

The measured spectra for the rod alone case and the rod-airfoil case both feature a strong tonal component corresponding to the frequency of shedding of the Kármán vortices by the rod. The presence of the airfoil increases the magnitude of emission peak of over 10 dB with respect to the rod alone case, in agreement with the measurements of Jacobs¹ and Casalino.² The peak shifts from 525 Hz to 500 Hz in presence of the airfoil. The latter phenomenon was also observed by Casalino, who ascribed it to a possible hydrodynamic-acoustic feedback induced by the airfoil onto the vortex release mechanism of the rod. The dashed (black) line indicates the spectrum of the background noise, which was shown in preliminary microphone array measurements to be mainly caused by the wind tunnel (see NLR report²⁴). This dominates the low frequency range for all the measurements up to approximately 200 Hz. Peaks starting at 500 Hz are generated by the acquisition system and have no physical relevance.

The spectra obtained as solution of the aeroacoustic analogy also exhibit a peak at 500 Hz. The magnitude of the peak shows good agreement with the measurement: 1 dB discrepancy for the full span coherence length (C.L. = 100 %) and 6 dB for half-span coherence (C.L. = 50 %). A similar pattern for the measured and the computed spectra is also observed in the narrow band between 300 and 500 Hz. The high frequency components exhibit the largest discrepancy with the microphone measurements. The assumption of in-phase coherence along a portion of the airfoil span, overestimates the emission due to small scale vortical structures, for which a shorter coherence length should be adopted. Improvements in the broadband noise prediction might derive from the application of a spanwise coherence model¹ tailored to the different characteristic lengths of the vortical structures or, more accurately, by the use of 3D flow data. Additional contributions to the mismatching are ascribed to 3D effects and experimental uncertainties in the evaluation of the pressure field. Furthermore the eventual amplification or cancelation of the acoustic pressure at the microphone position due to the rod emission (see Casalino²⁶) could not be evaluated by the present computation.

The aerodynamic forces have been evaluated on the control volumes CV (indicated in the bottom left

picture of Figure 3) at a distance from the LE normalized with the airfoil chord (d/chord) corresponding to 0.2 and aspect ratio of 5. The spectrum calculated with the integral formulation (triangle-label, orange line) shows a similar trend with respect to the distributed formulation. For the same correlation length (C.L. = 50 %) the integral approach exhibits overall magnitude levels of about 5 dB higher. The reason for this is currently ascribed to an overestimation of the loads calculated with control volume integration. Assessment on the accuracy of the loads determination method for the rod-airfoil configuration requires further analysis. From an experimental point of view this method offers the advantage of avoiding the direct pressure determination at the airfoil surface (see van Oudheusden¹⁹).

Equation (1) has been evaluated on the plane of the airfoil midspan at a distance from 1.25 m (where the microphones are located) to 2.25 m, for 90 angular locations ($\Delta\theta = 4^\circ$), allowing the visualization of the propagating wavefronts. Figure 7 shows a time sequence of the acoustic propagation.

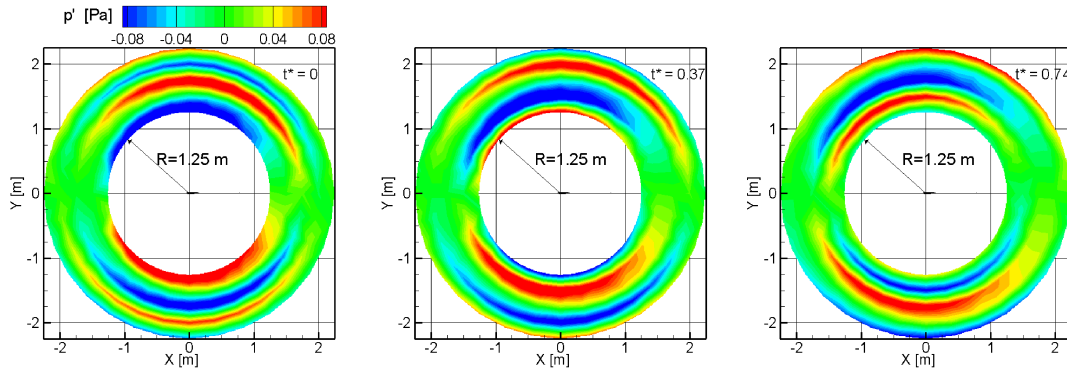


Figure 7. Time sequence of the radiated pressure fluctuation p' at normalized times t^*

The main emission appears to be perpendicular to the airfoil chord. The wavefronts represented by stripes of the same color are spaced by a distance of approximately 0.6 m, which corresponds to one acoustic wavelength at the shedding frequency. The quantitative evaluation of the directivity pattern at 1.25 m distance is provided by the polar plot of Figure 8. The OASPL of the computed spectra is evaluated between 200 and 1350 Hz (Nyquist cutoff). The angle 0° indicates the upwind direction and the angle 90° the direction perpendicular to the chord on the airfoil midspan plane. The green circles indicate the OASPL measured by the four far-field microphones of Figure 1 (right), evaluated on the same bandwidth. The OASPL measured by the microphone at $\theta = 90^\circ$ is fitted to the value obtained by the aeroacoustic prediction at the same position in order to provide a direct comparison of the angular decay.

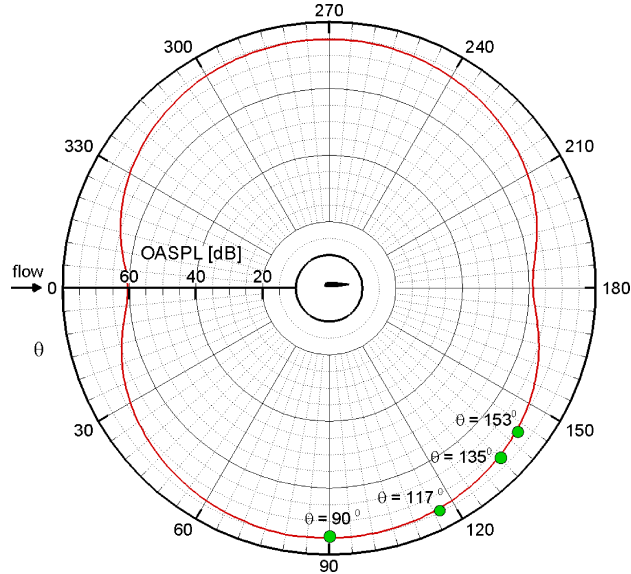


Figure 8. Polar plot of the computed OASPL and measured OASPL at four microphone positions (green circles)

The emission directivity exhibits a maximum intensity along the direction perpendicular to the airfoil chord and a reduction of about 20% in the streamwise direction. The angular decay of the measured OASPL indicated by the green circles, shows good agreement with the values obtained by Curle's analogy based on the PIV measurements.

V. Conclusion

The feasibility of using time-resolved PIV for the aeroacoustic prediction of a rod-airfoil configuration noise was investigated. The velocity fields around the airfoil measured by TR-PIV were used to calculate the unsteady pressure field by means of 2D spatial integration of the Poisson equation. The pressure evaluated on the solid surface constituted the source term according to Curle's formulation. Additionally a more straightforward integral approach based on the evaluation of the aerodynamic loads was followed for comparison. The acoustic predictions were compared with far-field microphone measurements at corresponding locations. It has been observed that the source of the acoustic emission is concentrated in the first 20 % of the airfoil surface where vortex-surface interaction produces the strongest unsteady pressure fluctuations.

The computed spectra revealed good agreement with the microphone measurements for the tonal component and the narrow frequency band below the peak, with a confidence level within 10 %, varying with the assumed spanwise correlation length. Larger discrepancies are observed at high frequencies which are ascribed to the choice of a single spanwise coherence length for all flow scales. Further uncertainties are to be evaluated with respect to 3D effects and temporal resolution. Possible improvements in the evaluation of the broadband component may be obtained by using 3D Tomographic PIV.²⁷ The spectrum obtained by the integral loads formulation reveals a good agreement with the distributed formulation in terms of spectral composition although the magnitude level are about 8% higher. An accuracy assessment of the loads determination method based on control volume integration for the present configuration is required. The latter method would present considerable advantages from an experimental point of view.

The present investigation revealed that PIV approaches are suitable for the prediction of the main features of the vortex structure interaction noise provided that the requirements on spatio-temporal resolution and 3D flow visualization can be met by the measurement apparatus. It remains to be explored the possible development of such approach for more general turbulent flow-surface interaction problems of broadband nature. The possible utilization of three-dimensional PIV by means of tomography opens the perspective to use also 3D-time resolved data as an input to acoustic analogies and for source identification.

Acknowledgments

This work is carried out within the FLOVIST project (Flow Visualization Inspired Aeroacoustics with Time Resolved Tomographic Particle Image Velocimetry) funded by the European Research Council (ERC) grant # 202887. Dr. Christophe Schram and prof. Mico Hirschberg are acknowledged for the insightful comments.

References

- ¹Jacob, M. C., Boudet, J., Casalino, D., and Michard, M., "A rod-airfoil experiment as benchmark for broadband noise modeling," *Theoretical and Computational Fluid Dynamics*, Vol. 19, 2004, pp. 171–196.
- ²Casalino, D., Jacob, M., and Roger, M., "Prediction of rod-airfoil interaction noise using the Ffowcs-Williams-Hawkings analogy," *AIAA*, Vol. 41, No. 2, 2003, pp. 182–191.
- ³Jacob, M., Ciardi, M., Gamet, L., Greschner, B., Moon, Y. J., and Vallet, I., "Assessment of CFD broadband noise predictions on a rod-airfoil benchmark computation," *AIAA*, 2008-2899, 2008.
- ⁴Seiner, J. M., "A new rational approach to jet noise reduction," *Theoretical and Computational Fluid Dynamics*, Vol. 10, 1997, pp. 373–383.
- ⁵Seiner, J. M. and K., P. M., "Jet noise measurements using PIV," *5th AIAA/CEAS Aeroacoustic Conference*, Vol. AIAA-99-1869, 1999.
- ⁶Goldstein, M. E., *Aeroacoustics*, McGraw-Hill, New York, 1976.
- ⁷Wernet, "Temporally resolved PIV for space-time correlations in both cold and hot jet flows," *Measurement Science and Technology*, Vol. 18, 2007, pp. 1387–1403.
- ⁸Schröder, W., Dierksheide, U., Wolf, J., Herr, M., and Kompenhans, J., "Investigation on trailing-edge noise sources by means of high-speed PIV," *12th international Symposium on Application of Laser Techniques to Fluid Mechanics*, 2004.
- ⁹Howe, M. S., "Trailing edge noise at low Mach numbers," *Journal of Sound and Vibration*, Vol. 225, 1999, pp. 211–238.
- ¹⁰Henning, A., Kaepernick, K., Ehrenfried, K., Koop, L., and Dillman, A., "Investigation of aeroacoustic noise generation by simultaneous particle image velocimetry and microphone measurements," *Experiments in Fluids*, Vol. 45, 2008, pp. 1073–1085.
- ¹¹Schram, C., Taubitz, S., Anthoine, J., and Hirschberg, "Theoretical/empirical prediction and measurement of the sound produced by vortex pairing in a low Mach number jet," *Journal of Sound and Vibration*, Vol. 281, 2005, pp. 171–187.
- ¹²Powell, A., "Theory of vortex sound," *Journal of the Acoustical Society of America*, Vol. 36, No. 1., 1964, pp. 177–195.
- ¹³Möhring, W., "On vortex sound at low Mach number," *Journal of Fluid Mechanics*, Vol. 85, 1978, pp. 685–691.
- ¹⁴Haigermoser, C., "Application of an aeroacoustic analogy to PIV data from rectangular cavity flow," *Experiments in Fluids*, 2009, 00348-009-0642-5.
- ¹⁵Lighthill, M. J., "On sound generated aerodynamically, Part I: General theory," *Proc. Roy. Soc. Lon.*, Vol. A 211, 1952, pp. 564–587.
- ¹⁶Curle, N., "The influence of solid boundaries upon aerodynamic sound," *Proc. Roy. Soc. Lon.*, Vol. A 231, 1955, pp. 505–514.
- ¹⁷Wang, M., Freund, J. B., and Lele, K. L., "Computational prediction of flow-generated sound," *Annual review of Fluid Mechanics*, Vol. 38, 2006, pp. 483–512.
- ¹⁸Kurtulus, D. F., Scarano, F., and David, L., "Unsteady aerodynamics forces estimation on a square cylinder by TR-PIV," *Experiments in Fluids*, Vol. 42, 2007, pp. 185–196.
- ¹⁹van Oudheusden, B. W., "PIV-based forces and pressure measurements," *Recent advances in Particle Image Velocimetry*, Vol. LS 2007-09, von Karman Institute, Rhode-St-Genève, 2009.
- ²⁰Liu, X. and Katz, J., "Instantaneous pressure and material acceleration measurements using a four-exposure PIV system," *Experiments in Fluids*, Vol. 41, 2006, pp. 227–240.
- ²¹de Kat, R., van Oudheusden, B. W., and Scarano, F., "Instantaneous planar pressure field determination around a square-section cylinder based on time-resolved stereo PIV," *14th Int Symposium on the Application of Laser Techniques to Fluid Mechanics*, Lisbon, Portugal, July 2008.
- ²²Scarano, F. and Riethmuller, M. L., "Iterative multigrid approach in PIV image processing," *Exp.Fluids*, Vol. 26, 1999, pp. 513–523.
- ²³Roger, M. and Moreau, S., "Trailing edge measurements and prediction for subsonic loaded fan blades," *AIAA 2002-2460*, Vol. 85, 2002.
- ²⁴Lorenzoni, V., Tuinstra, M., and Scarano, F., "Combined PIV and acoustic measurements on a rod-airfoil configuration. Pilot test of the FLOVIST project," Tech. rep., Nationaal Lucht-en Ruimtevaart laboratorium (NLR), 2008.
- ²⁵Lorenzoni, V., *Aeroacoustic investigation of rod-airfoil noise based on time-resolved PIV*, Master's thesis, TU Delft, 2008.
- ²⁶Casalino, D., *Analytical and numerical methods in vortex-body aeroacoustics*, Ph.D. thesis, Politecnico di Torino et L'École Centrale de Lyon, 2002.
- ²⁷Elsinga, G. E., Scarano, F., Wieneke, B., and van Oudheusden, B. W., "Tomographic particle image velocimetry," *Exp. Fluids*, Vol. 41, 2006, pp. 933–947.